Journal of Structural Geology 33 (2011) 690–697

Contents lists available at ScienceDirect

Journal of Structural Geology

journal homepage: www.elsevier.com/locate/jsg

Modelling partially-emptied compaction bands induced by borehole drilling

R. Katsman [a,*], B.C. Haimson [b]

[a] The University of Haifa, Faculty of Science and Science Education, The Dr. Moses Strauss Department of Marine Geosciences, Mount Carmel, Haifa 31905, Israel
[b] University of Wisconsin–Madison, Department of Materials Science and Engineering, and the Geological Engineering Program, 1509 University Ave., Madison, WI 53706-1595, USA

ARTICLE INFO

Article history:
Received 13 January 2010
Received in revised form
4 January 2011
Accepted 21 January 2011
Available online 27 January 2011

Keywords:
Compaction band
Borehole breakout
Borehole drilling
Rock mechanics
True triaxial testing

ABSTRACT

Drilling into rock blocks subjected to critical far-field stresses can result in localized failure around the created borehole, manifested by the formation of two diametrically opposed breakouts. In weakly bonded quartz-rich porous sandstones breakouts take the form of narrow tabular (slot-like) openings extending along a plane perpendicular to the maximum applied-stress direction. SEM images strongly suggest that these breakouts are compaction bands (CB's) that have been emptied to different degrees. Debonded grains, some whole, others cracked or crushed, within the compaction band are totally or partially removed by the circulating drilling fluid, creating the breakout. A new analytical model is developed here, which computes the stress field around partially-emptied CBs and predicts the expected lengths of these defects and their dependence on borehole radius and the extent of the CB emptying by the drilling fluid. It is found that boreholes with larger radius generate longer partially-emptied CBs. The results also demonstrate that when the ratio of the filled to the emptied part of a CB increases (addressing a smaller drilling fluid flow rate), the resulting total length of partially-emptied CB decreases. Both of these findings are in good agreement with results of drilling experiments conducted by Sheets and Haimson (2004).

1. Introduction

The Earth's crust is subjected to in situ stresses predominantly resulting from gravitational and tectonic forces. Crustal principal stresses, especially at depths greater than several hundred meters, act typically in the vertical direction and the horizontal plane. Drilling vertically into the Earth's crust introduces a cylindrical discontinuity in the rock mass, which brings about at any given depth a constant low radial stress at the borehole wall, and a concentrated tangential stress that varies with the angular position. The increased difference between tangential and radial stresses at angles approaching the direction of the minimum horizontal far-field stress may result in failure in the form of borehole breakouts. Boreholes drilled into the Earth's crust for facilitating the extraction of water, petroleum, natural gas, geothermal steam, or for enabling geophysical observations, can reach depths of several kilometers, where in situ stresses are high and rock formations can be rather weak. During or immediately after drilling, boreholes often develop 'breakouts' as a consequence of stress-induced rock failure. Field observations and laboratory test results have supported theoretical findings that in vertical boreholes breakouts develop along a plane perpendicular to the maximum horizontal far-field stress σ_1 (see for example Haimson, 2007).

Laboratory tests also revealed that the breakout span at the intersection with the borehole wall is directly related to the state of the far-field stress (Song and Haimson, 1997). Vernik and Zoback (1992), Brudy et al., (1997), Haimson and Chang (2002), and Haimson et al. (2010), successfully utilized logged breakout spans and known rock criteria of failure to estimate the maximum horizontal in situ stress, σ_1, in the deep scientific vertical holes of Cajon Pass, California, KTB, Germany, and in the vicinity of Chelungpu Fault, Taiwan.

Using microscopic observations, Haimson (2007) distinguishes between two major types of breakouts. In low-porosity rock (granite, limestone, and well-cemented arkosic sandstone) critical stresses at the points of intersection of the diameter aligned with σ_3 direction and the borehole perimeter (Fig. 1) lead to brittle failure in the form of intra- and trans-granular densely-spaced dilatant microcracking parallel to σ_1 and along the σ_3 springline, giving rise to V-shaped (dog eared) breakouts.

However, in medium to high-porosity (10–30%) quartz-rich sandstones, which typically have weakly suture-bonded grains, borehole failure takes the shape of narrow, tabular (slot-like)

* Corresponding author. Tel.: +972 523761001.
E-mail addresses: reginak@research.haifa.ac.il (R. Katsman), bhaimson@wisc.edu (B.C. Haimson).

0191-8141/$ – see front matter © 2011 Elsevier Ltd. All rights reserved.
doi:10.1016/j.jsg.2011.01.010

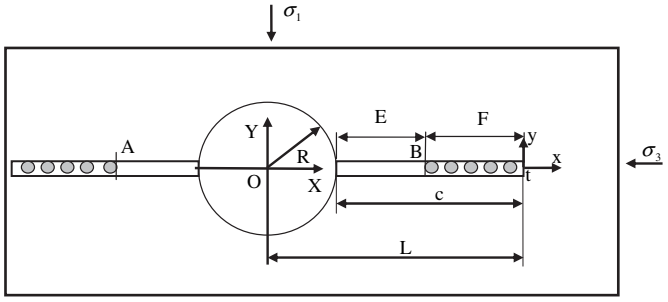

Fig. 1. During or immediately after drilling in high-porosity sandstones, boreholes often develop 'slot-like breakouts' as a consequence of stress-induced compactive rock failure. The loosened grains and fragments accumulated within the compaction band (CB) emerging from the borehole are ejected from the CB into the borehole either on their own or/and with the help of the circulating drilling fluid. At intermediate flow rates (~0.03L/s) the amount of compacted and loosened grains removed by the circulating fluid constitutes only a partial emptying (denoted by E) of the CB emanating from a borehole. However, the rest of the breakout (denoted by F) remains filled with compacted and loosened (and sometimes crushed and shattered) grains.

breakouts extending along a direction perpendicular to σ_1 (Fig. 1). Experimental evidence suggests that the high compressive stresses in the plane normal to σ_1 bring about the debonding of a narrow band of grains, often accompanied by grain splitting, shattering, and porosity reduction occurring without recognizable shear offset. An example of porosity reduction, along a narrow strip ahead of the breakout tip in Mansfield sandstone is shown in Fig. 2. See also Haimson and Song (1998), Haimson and Klaetsch (2007), Haimson and Kovacich (2003), Sheets and Haimson (2004). This damaged zone was analyzed by microstructural observations and is found to be remarkably similar to a compaction band or 'CB', the feature discerned in the field by Mollema and Antonellini (1996), and further observed in situ by Sternlof et al., (2005). Discrete CBs were further reproduced experimentally in initially intact sandstone samples (e.g. Klein et al., 2001; Townend et al., 2008), and in notched samples (e.g. Vajdova and Wong, 2003; Vajdova et al., 2003).

A survey of the literature on other rock mechanics experiments on high-porosity sandstones in which breakouts were observed, points to two recent studies (Cuss et al., 2003; Dresen et al., 2010). Their tests were conducted on cylinders with pre-drilled axial holes subjected to hydrostatic loading (i.e. one in which all principal stresses are equal). Unlike our tests, they did not intend to simulate in situ conditions in which commonly the state of stress is anisotropic (three different principal stresses) and where boreholes or wells are drilled in rock already subjected to the prevailing state of stress. Cuss et al. and Dresen et al. did not observe clear slot-shaped breakouts, like those obtained in our tests. This can be attributed to the fact that such features have only been realized in rectangular samples subjected to highly differential far-field principal stresses acting in planes perpendicular to the borehole axis.

Katsman et al. (2006a) and Katsman et al. (2006b) proposed to characterize CBs as Localized Volume Reduction (LVR) features resulting from the localized plastic strain produced by mechanical compaction. The stresses in the vicinity of the CB were calculated both analytically and numerically (Katsman et al., 2006a; 2006b) and a good agreement between the solutions was demonstrated. Addressing the nucleation of CBs near defects of different nature, like cracks, notches (Vajdova and Wong, 2003; Vajdova et al., 2003), and previously created CBs, a new numerical model was created (Katsman and Aharonov, 2006), and results of the simulations were found to be in agreement with experimental observations. The numerical simulations showed that the compaction process is initiated by compressive stress concentrations, existing in the vicinity of defects (cracks, initial CBs, holes).

Haimson and Kovacich (2003) and Sheets and Haimson (2004), investigated the effect of different drilling parameters on the occurrence of slot-shaped breakouts in high-porosity quartz-rich Berea and Mansfield sandstones. They demonstrated that slot-breakout length is directly correlatable to the magnitude of σ_1; while higher flow rates of the circulating drilling fluid improve the efficiency of the CB loosened grain removal, thus extending breakout length.

The two extreme cases, one of totally emptied CB created under high fluid flow rate, 0.06L/s or more (Haimson and Kovacich, 2003), and the other of practically filled (or un-emptied) CB created under low fluid flow rate, 0.01L/s or less (Haimson and Kovacich, 2003; Sheets and Haimson, 2004) were studied analytically in Katsman et al., (2009). A new model was developed in order to compute the stress field around totally emptied/filled CBs and determine factors affecting final breakouts lengths. It was shown that unlimited growth of empty defects, like cracks or emptied CBs, is caused by the inability of these defects to transmit the applied load under either compression or extension, thus causing the stress at their tips to grow as they elongate. In contrast, volume reduction defects, such as filled CBs, do transmit the applied load. They are characterized by a constant stress at the vicinity of their tip, thus restricting their growth and final length. Hence, filled CBs emanating from borehole walls have very limited length and are therefore always shorter than the emptied ones, under otherwise equal experimental conditions. Next, it was demonstrated that presence of a borehole also affects the total stress field around emptied/filled defects. In addition, it was shown that definite correlations exist between borehole breakout dimensions and in situ stress magnitudes, specifically the main principal stress, σ_1, the feature observed also in laboratory experiments (Haimson, 2003; Haimson and Kovacich, 2003; Sheets and Haimson, 2004; Haimson and Klaetsch, 2007). The new model demonstrated a very good agreement with the experimental results of Haimson and co-workers (Haimson and Kovacich, 2003; Sheets and Haimson, 2004).

This paper studies parameters affecting the final length of CBs created at borehole walls by focusing on partially-emptied CBs, which are commonly observed in experiments at intermediate flow rates (between 0.01L/s and 0.06L/s) (Haimson and Kovacich, 2003; Sheets and Haimson, 2004). The influence of the following parameters on the final partially-emptied CB lengths is studied:

- The borehole radius.
- The extent of CB emptying as affected by the fluid flow rate. The designed model does not simulate fluid flow explicitly. It is assumed that greater flow rate is capable of emptying a larger part of the CB and thus of decreasing the proportion of the filled segment (F) to the emptied one (E) (F:E) and vice versa (Fig. 1). We therefore explore how the different ratios F:E (Fig. 1) affect the final length of the partially-emptied CB.

The new analytical model presented here is built upon the model developed in Katsman et al., (2009), and relies on our previous works (Katsman et al., 2006a, 2006b).

2. Summary of experimental work

2.1. Experimental Setup and procedure

The laboratory drilling experiments carried out at the University of Wisconsin have been described in detail by Haimson (2003). Central vertical holes (normally 20 mm in diameter) are drilled in rock blocks, typically of size 150 × 150 × 230 mm, subjected to preset true triaxial far-field stresses generated by compressive loads applied to their surfaces. The vertical (σ_2), and the maximum

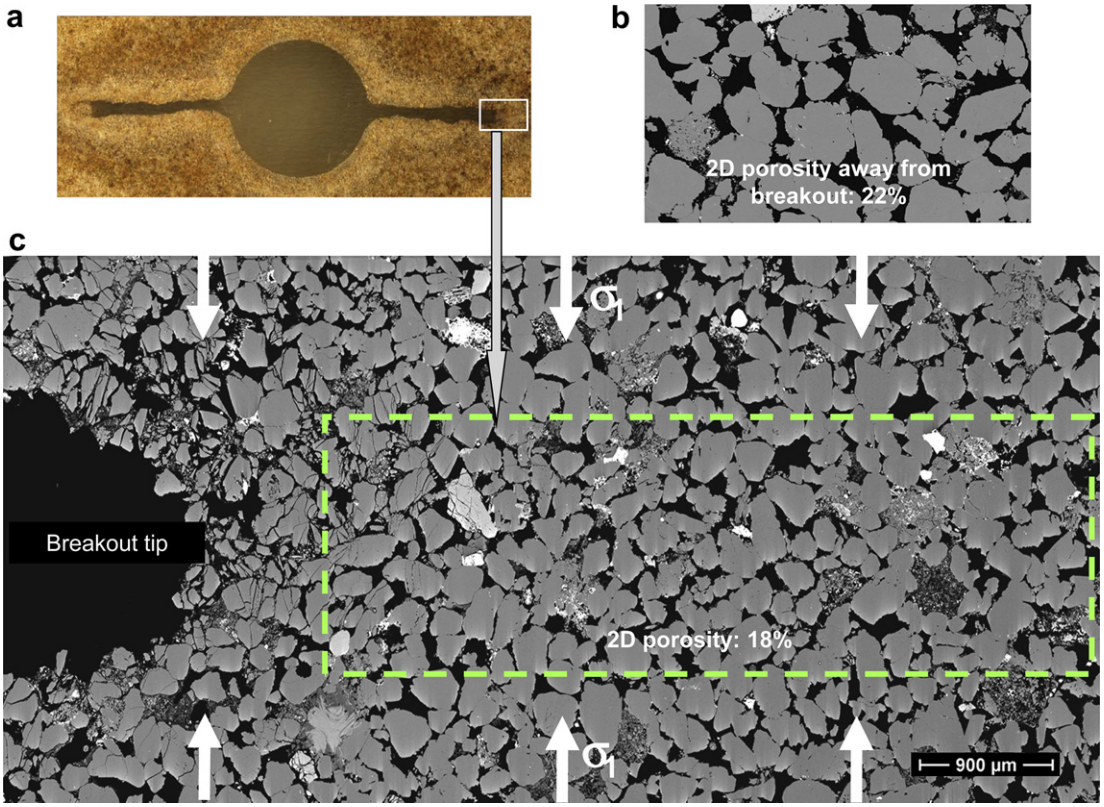

Fig. 2. (a) A slot-like breakout near borehole in Mansfield sandstone. (b) The 2D porosity as determined from the pore projection onto the plane under the scanning electron microscope (SEM) is 22%. A SEM view of the breakout tip (c) reveals that the strip of grains ahead of it and possessing the same width as the breakout has a reduced porosity (18%), as expected from a compaction band (this one having developed as a result of drilling the borehole in a pre-stressed medium with the maximum principal stress (σ_1) acting in the direction shown).

and minimum horizontal principal stresses (σ_1 and σ_3) are all unequal and of magnitudes typical of crustal conditions. Drilling fluid (usually tap water), is circulated at a prescribed flow rate (usually between 0.01L/s and 0.06L/s, Haimson and Kovacich, 2003; Sheets and Haimson, 2004) through the borehole as it is created, evacuating the debris created by the drilling operation. When breakouts are induced during drilling, the circulating fluid flushes out debonded grains and fragments from within the breakout. At the conclusion of drilling the borehole is immediately filled with epoxy to preserve borehole wall conditions. Cross sections of the tested blocks are then studied to determine breakout geometry and orientation. Optical and scanning electron microscopes (SEM) are used to observe the grain-scale mechanism leading to breakout formation (e.g. Fig. 2).

2.2. Rock types and experimental results

The model discussed here simulates the tests conducted on Mansfield sandstone (Sheets and Haimson, 2004). The rock has a porosity in excess of 20%, is quartz-rich, with grains that are predominantly bonded by weak suturing and by little or no cementing material. Table 1 presents some physical and mechanical properties of Mansfield sandstone as determined in the University of Wisconsin rock mechanics laboratory (Sheets and Haimson, 2004). Generally, breakouts were slot-shaped and several grain diameters wide. They extended along a plane perpendicular to the major horizontal principal stress, (Fig. 1). In this paper we focus only on some of the experimental results in this rock, those in which the breakouts can be considered partially-emptied CBs (Fig. 1).

3. Model

This section describes the analytical model created to predict the length of partially-emptied CBs under various degrees of emptying depending on the fluid flow rate, various borehole diameters, and different far-field applied stresses (Fig. 1).

3.1. Stresses

The variable that determines whether CBs are arrested or progressively lengthened is the level of stress concentration at their tip (point t, Fig. 1), (Katsman et al., 2009). Similar to the cases studied in Katsman et al. (2009), the enhanced stress at the tip of

Table 1
Physical and mechanical properties of Mansfield sandstone.

Properties	Mansfield sandstone
Mineral composition	Quartz 90%, mica 7%
Primary grain bonding	Sutured grain contacts
Uniaxial compressive strength	19.3 MPa
Brazilian tensile strength	1.1 MPa
Rock cohesion	8.4 MPa
Internal friction angle	41°
Porosity 3d	27%
Porosity 2d	22%
Porosity 2d after comp.	17.9%
Poisson ratio	0.25
Band's half-width after compaction, h	1.15 mm
Young's modulus	9.6 GPa
Grain diameter	0.24 mm
Borehole radius	11.5 mm
ΔP excess fluid pressure	0.4 MPa

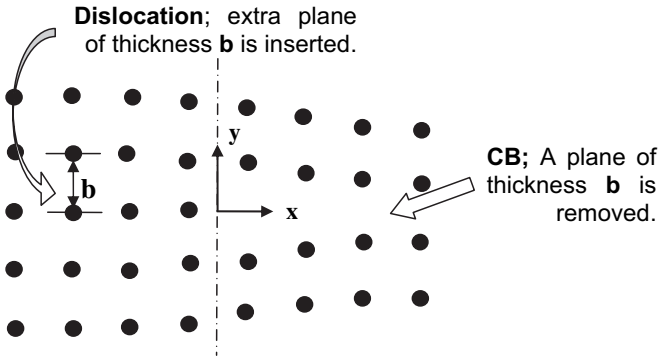

Fig. 3. Compaction band formation interpreted in terms of edge-dislocations. Edge dislocations are constructed by insertion of an "extra" half-plane, of thickness b, into an elastic body. In contrast, a compaction band is constructed by removal of a half-plane of thickness b from an elastic body.

the partially-emptied CB emanating from the borehole (point t, Fig. 1), arises from a combination of (1) the stress induced by the filled part of CB (part *F*, Fig. 1) and (2) the stress induced by the emptied part of CB including the borehole (part *E* and the borehole itself, Fig. 1).

We consider a borehole drilled vertically into the earth's crust, parallel to the principal stress (σ_2). The other two principal stresses (σ_1,σ_3 , Fig. 1) are horizontal and are specified as loading boundary conditions at infinity. Under these conditions the strain in the vertical *Z* direction is constant, $\epsilon_{zz} = \partial w/\partial z = \epsilon = const$, where the vertical displacement *w* is independent of *X* and *Y*, the horizontal axes. In this case, σ_{xx} and σ_{yy} depend only on *X* and *Y*, as under either plane strain or generalized plane stress conditions (Jaeger and Cook (1976), Section 5.3, case vii).

We analyze the 3D stress field for two configurations: (1) filled part of CB (part *F*, Fig. 1), and (2) emptied part of CB emanating from a borehole (part *E* and the borehole, Fig. 1). The stress fields around emptied and filled defects are completely different (Katsman et al., 2006a, 2006b, 2009). The stress around an emptied CB (Part *E*, Fig. 1) is associated with that of a Mode I flaw under compression (see Katsman et al., 2006a), where the stress around the defect tips compensates for stresses unsupported by the empty defect. In contrast, the stress around a filled CB, (part *F*, Fig. 1) is produced by the irreversible plastic strain as a result of grain crushing and porosity reduction generated by mechanical compaction.

3.1.1. Stresses around a filled segment of CB

The filled part of a CB extends from point B to point t in Fig. 1. Following the theoretical and numerical study of Katsman et al. (2006b), the stress in the vicinity of a filled CB is identical to that of an edge dislocation, which can be constructed by insertion of an "extra" plane, of width *b* (in the *Y* direction), into an elastic lattice of atoms (Fig. 3). In a macroscopic analogy, a CB is constructed by removing a plane of width *b* and length *2c*, from an elastic body (Fig. 4), where

$$b = 2(H - h) \tag{1}$$

with *H* defined as the half-width of the CB material before it underwent compaction, and *h* is the CB half-width after compaction, Fig. 4, and Table 1. The plastic strain that is accommodated by the compaction process within a CB, *b/2H,* may be calculated from the porosity reduction that occurred within the CB, using Eq. (3) in Katsman and Aharonov (2006):

$$\frac{b}{2H} = \frac{\phi_{\text{init}} - \phi_{\text{comp}}}{1 - \phi_{\text{comp}}} \tag{2}$$

b is thus calculated from Eqs. (1) and (2) using the CB half-width, *H*, and the initial and final porosities, ϕ_{init}, and ϕ_{comp} (Table 1). Having obtained *b*, the stresses around a CB may be calculated using the formulation outlined in Katsman et al. (2006b). Since the stresses around a CB are nearly independent of its length, we use the half-infinite approximation:

$$\sigma_{xx}^{CB} = -bA\frac{x(y^2 - x^2)}{(y^2 + x^2)^2} \tag{3a}$$

$$\sigma_{yy}^{CB} = bA\frac{x(3y^2 + x^2)}{(y^2 + x^2)^2} \tag{3b}$$

$$\sigma_{xy}^{CB} = -bA\frac{y(y^2 - x^2)}{(y^2 - x^2)^2} \tag{3c}$$

$$A \equiv \frac{\mu}{2\pi(1 - \nu)} \tag{3d}$$

where μ is shear modulus, and ν is Poisson's ratio of Mansfield Sandstone (Sheets and Haimson, 2004) (Table 1). Here the origin of the coordinates, t(*x*, y), is positioned at the CB tip, Fig. 1. Therefore *x* is defined as $x = X - L$, where *L* is a distance from the borehole center to the CB tip, *t*. Compressive stresses are assumed to be positive.

The stress responsible for the propagation of a CB is the stress right at its tip at point t ($x = 0$). However, the stress at that point ($x \to 0$, $y = 0$) predicted analytically is singular, similar to the singularity arising at crack tips. To avoid this singularity (Scholz, 2000) one may define the tip stress as the stress at some small distance x_0 from the CB tip (along $y = 0$), defined as a compactive process zone length and discussed in Section 3.3 (see also Tembe et al., 2006; Katsman et al., 2009).

Inserting $x \to x_0$, $y = 0$ into Eqs. (3a–3c), we obtain the following stress components at the tip of the filled segment of CB:

$$\sigma_{xx}^{f}(tip) = \sigma_{yy}^{f}(tip) = A\frac{b}{x_0} \tag{4a}$$

$$\sigma_{xy}^{f}(tip) = 0 \tag{4b}$$

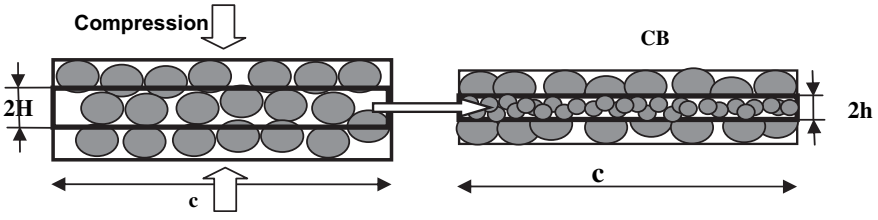

Fig. 4. Localized volume reduction accompanying compaction band formation in a high-porosity rock. The process is characterized by vertical shortening (2H- before compaction, 2 h- after compaction), with no lateral dimensional changes (c- the length of the band before and after compaction).

3.1.2. Stresses around an emptied segment of a CB emanating from a borehole

The emptied part of the CB emanating from a borehole is presented in Fig. 1 by segment *E*. It has been shown that flaws whether in extension or compression produce equivalent stress fields, differing in signs only (e.g., Katsman et al., 2006b). We consider empty CBs as geometrically equivalent to slot-shaped cracks under compression. Thus, the horizontal stress components, σ_{xx} and σ_{yy} along $Y = 0$, in the vicinity of a slot-like empty CB adjacent to a borehole, are equal to stresses in the vicinity of a Mode I slot-like crack placed under constant strain conditions (in *Z* direction):

$$\sigma^e_{xx} = \sigma^e_{yy} = \frac{K_I}{\sqrt{2\pi\omega}} \tag{5a}$$

$$\sigma^e_{xy} = 0 \tag{5b}$$

where ω is a distance (including also the process zone length, x_0) from the emptied segment tip (point B, Fig. 1) along *X* axis to the tip of the filled part of CB (point t, Fig. 1), the point where the tip stresses responsible for the CB propagation are calculated: $\omega = F + x_0$ (see Fig. 1). K_I is the stress-intensity factor in *Mode I* loading. For the specific configuration including borehole and two slot-shaped cracks emanating from it depicted in Fig. 1, the stress-intensity factor is formulated in the Murakami's 'Stress intensity factors handbook' (Murakami, 1987):

$$K_I = F_{tab}\sigma_1\sqrt{\pi(R+E)} \tag{5c}$$

where F_{tab} is a tabulated function depending on the loading conditions, and the relation between the borehole radius and the breakout length; $(R + E)$ is the distance from borehole center (point *O*) to the emptied CB tip (point *B*).

3.1.3. Total stresses around a partially-emptied CB emanating from a borehole

The horizontal stress components at the tip of a partially-emptied CB that emanates from a borehole (point t, Fig. 1) are a linear combination of (1) the stress at that point induced by the filled part of the CB (Eq. (4)), and (2) the stress induced by the emptied part of the CB adjacent to a borehole, (Eq. (5)):

$$\sigma_{xx} = \sigma^e_{xx} + \sigma^f_{xx} \tag{6a}$$

$$\sigma_{yy} = \sigma^e_{yy} + \sigma^f_{yy} \tag{6b}$$

$$\sigma_{xy} = \sigma^e_{xy} + \sigma^f_{xy} = 0 \tag{6c}$$

The vertical stress component σ_{zz} at the CB tip under the considered constant strain conditions ($\epsilon = const \neq 0$) is a function of σ_{xx} and σ_{yy} (Eq. (6)): $\sigma_{zz} = E\epsilon + \nu(\sigma_{xx} + \sigma_{yy})$ (Eq. (22), Section 5.4, in Jaeger and Cook, 1976), while on a macro-scale $E\epsilon = \sigma_2 - \nu(\sigma_1 + \sigma_3)$.

Therefore, combining Eqs. (5, 6), and the above basic equations from Jaeger and Cook (1976):

$$\sigma_{zz} = 2\nu\left[\left(-\frac{\sigma_1+\sigma_3}{2}\right) + \frac{K_I}{\sqrt{2\pi(F+x_0)}} + A\frac{b}{x_0}\right] + \sigma_2 \tag{6d}$$

and

$$\sigma_{xz} = \sigma_{yz} = 0 \tag{6e}$$

3.2. The yield function, f

After computing the stresses at the tip of the partially-emptied CB, we predict how long this defect will turn out to be. When stress components at the tip of the partially-emptied CB (Eq. (6)) attain the critical values specified by an appropriate yield criterion, localized compaction will occur. The choice of the yield function is described in Katsman et al., (2009). Here this matter is presented in brief. Following Tembe et al. (2006) and Baud et al. (2006), the material yield function f in the σ_{ij} stress field is formulated as a function of the first two stress invariants I_1 and J_2:

$$I_1 = (\sigma_{xx} - P_p) + (\sigma_{yy} - P_p) + (\sigma_{zz} - P_p) \tag{7a}$$

$$J_2 = \left[(\sigma_{xx}-\sigma_{yy})^2 + (\sigma_{yy}-\sigma_{zz})^2 + (\sigma_{zz}-\sigma_{xx})^2\right] \Big/ 6 + \sigma^2_{xy} + \sigma^2_{yz} + \sigma^2_{xz} \tag{7b}$$

and is independent of the third stress invariant (Wong et al., 1997; Baud et al., 2006).

The constitutive model considered here, and in Katsman et al. (2009), adopts a yield function of the form:

$$f(\sigma_{ij}) = \frac{(I_1 - c)^2}{a^2} + \frac{J_2}{b^2} - 1 = 0 \tag{8}$$

which corresponds to an ellipse centered at (c,0) with major and minor semi- axes of *a* and *b* (Baud et al., 2006). The parameters *a, b*, and *c* for the yield envelope of the specific Mansfield Sandstone studied here (Table 1) are not available in the literature. They are estimated from Baud et al. (2006) considering a rock similar to Mansfield Sandstone in its quartz content. This rock is the Bentheim Sandstone, whose properties were evaluated by Baud et al. (2006), and presented here in Table 2. Parameters *a, b*, and *c* relate to *A, B*, and *C* formulated for the Critical State Model in Baud et al. (2006) (Table 3 therein), as A = a/3, B = $\sqrt{3}$b, and C = c/3.

If $f(\sigma_{ij}) \geq 0$, localized compaction is expected to occur, leading to CB formation and propagation, however if $f(\sigma_{ij})$ drops below zero, CB propagation is arrested (Baud et al., 2006). As the stress field at the defect tip is responsible for the defect propagation, we assume that the yield envelope described in Eq. (8) is applicable not only to large specimens (*18.4* × *38.1* mm) as in Baud et al. (2006), but also to the smaller scale of a defect tip with dimensions of process zone length, x_0. The intersection point of the $f(\sigma_{ij})$ curve with zero will predict the final breakout length, *c* (Fig. 1).

3.3. Compactive process zone length, x_0

When stresses at the tip of the partially-emptied CB attain the critical values specified by a yield criterion (Eq. (8)), compactive yield will initiate and spread over a compactive process zone, x_0, being a characteristic nucleation length-scale (Tembe et al., 2006). To approximate the dimensions of this process zone in 2D, a contour along which the yield function vanishes, $f(\sigma_{ij}) = 0$ (Eq. (8)), should be drawn around the defect tip (Tembe et al., 2006). Such a contour is encloses a 2D region of compactive damage. In our case, partially-emptied CBs emanating from the borehole in Mansfield sandstone is characterized by the uniform thickness (see Fig. 2). Therefore, the region of compactive damage is calculated in 1D presenting a "compactive process zone length", x_0.

Table 2
Physical properties and Critical State Model parameters for Bentheim sandstones (adopted from Baud et al., 2006).

Sandstone	Porosity, %	Grain Radius, mm	Amount of quartz, %	a, MPa	b, MPa	c, MPa
Bentheim	22.8	0.105	95	600	131	654

4. Results

This section compares predictions of expected partially-emptied CB lengths (Fig. 1), calculated using the analytical model described in Section 3, with the experimental results reported by Sheets and Haimson (2004) for the Mansfield Sandstone, for which properties are presented in Table 1. The influence of the following parameters on the partially-emptied CB lengths is studied:

i. The borehole radius.
ii. The extent of CB emptying (the ratio *F:E*, Fig. 1) as affected by the fluid flow rate. Large fluid flow rate decreases the proportion of the filled part (F) to the emptied one (E) and vice versa. The relation between the specific experimental flow rates and the resulting extent of CB emptying is not studied here, as fluid flow is not modeled in explicit form. We explore how the different ratios *F:E* affect the final length of the partially-emptied CB.

Parameters described above are varied in the model, analyzed below, and compared to the experimental results obtained by Sheets and Haimson (2004). Mansfield Sandstone properties are used in the calculations (Table 1). The Yield function $f(\sigma_{ij})$ is calculated using the Bentheim Sandstone parameters (Baud et al., 2006), (Table 2).

A trial process zone length, x_0 , was calculated for Mansfield Sandstone at several locations as the CB advanced, whereas no significant variability around $x_0 = 0.32$ mm was discerned (see also in Katsman et al., 2009). This value demonstrates a good agreement with the process zone length determined for the Bentheim sandstone, found both theoretically and experimentally (from microstructural observations) in Tembe et al. (2006).

4.1. Influence of the borehole radius

Boreholes of various diameters were drilled by Sheets and Haimson (2004), using an intermediate flow rate (approximately 0.03L/s, Fig. 7). When borehole radius in the experiments was changed, the flow rate was adjusted in order to maintain a constant fluid flow velocity within the annulus between the drill-bit and the borehole wall (Sheets and Haimson, 2004). This was done to ensure that the only variable tested was borehole size. It was verified in all the experiments that under this flow rate adjustment the ratio of the filled CB part to the emptied one (*F:E*, Fig. 1) remains approximately invariant, $F{:}E \cong 1$, at any borehole radius. This constant relation ($F{:}E \cong 1$) is used in the model as fluid flow is not modeled explicitly. The length of the partially-emptied CB (Fig. 1) for different borehole diameters is calculated for various loading conditions and compared to the length produced experimentally (Fig. 7, Sheets and Haimson, 2004).

The procedure of finding a final CB length (Fig. 5) is described in detail in Katsman et al. (2009). Here it is demonstrated for a representative loading conditions $\sigma_1 = 50$ MPa , $\sigma_2 = 30$ MPa, $\sigma_3 = 20$ MPa, and borehole radius $R_{bor} = 11.5$ mm, depicted in Fig. 7 (Sheets and Haimson, 2004) by the line with triangle markers. The applied far-field stresses (and also the applied far-field stresses specified in Fig. 6) agree with those estimated in situ by Sternlof et al. (2005) in an area of the extensive CBs exposure. Moreover, the stress field determined by Haimson et al. (2010) around the Chelungpu fault, Taiwan, also fits the prescribed loading well. A similar in situ state of stress in the Canadian Shield is noted by Brace and Kohlstedt (1980; Fig. 3), showing that at roughly 1400 m depth the vertical (σ_2) and the least horizontal (σ_3) stresses are around 30–35 MPa, but the maximum horizontal stress (σ_1) is between 55 and 75 MPa.

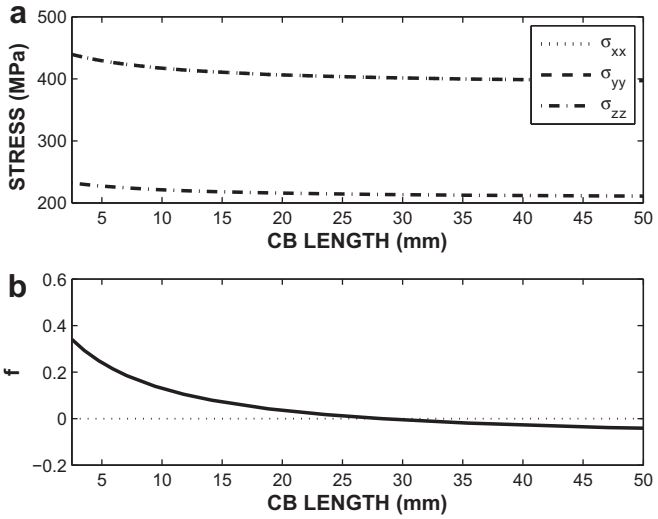

Fig. 5. Prediction of the final length of a partially-emptied compaction band developed in Mansfield Sandstone (Table 1) under specific applied stress conditions and borehole radius. The applied principal stresses are $\sigma_1 = 50$ MPa, $\sigma_2 = 30$ MPa, $\sigma_3 = 20$ MPa, and borehole radius is $R_{bor} = 11.5$ mm. σ_{xx}, σ_{yy}, and σ_{zz} are the stress components at the tip (t, Fig. 1) of a partially-emptied CB emanating from a borehole. f is the yield function for compaction. a) σ_{xx}, σ_{yy}, and σ_{zz} stress components are calculated from Eqs. (4–6) and plotted as a function of CB length. b) yield function $f(\sigma_{ij})$ is calculated from Eq. (8) using stress components depicted in Fig. 5a and Critical State Model parameters for Bentheim Sandstone (Baud et al., 2006, Table 2 here) as closest to the Mansfield Sandstone in Quartz content. Once $f(\sigma_{ij})$ falls down below zero, CB propagation stops. The predicted CB length is $c = 30.0$ mm.

σ_{xx}, σ_{yy}, and σ_{zz} are calculated from Eqs. (4–6) under these conditions, and plotted in Fig. 5a. The solid line in Fig. 5b is the calculated yield function $f(\sigma_{ij})$ (Eq. (8)) for Bentheim Sandstone (Baud et al., 2006, Table 2 here). Once $f(\sigma_{ij})$ falls below zero, CB propagation stops, thus producing a CB length of $c = 30$ mm. The experimentally measured CB length in Sheets and Haimson (2004), (their Fig. 7), yields also $c = 30$ mm. It can easily be demonstrated that calculated stress components (Fig. 5a) induce failure associated with right branch of the elliptic failure envelope (Fig. 4 in Baud et al., 2006) addressing compactive failure only.

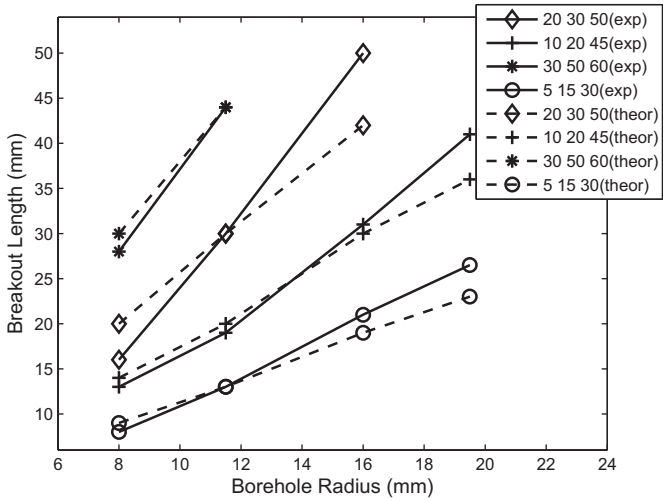

Fig. 6. Effect of the borehole radius on partially-emptied compaction band length. Compaction band lengths were calculated for different borehole radii under different loading conditions (dashed curves). The results are compared to the experimental results (solid lines) summarized in Fig. 7 of Sheets and Haimson (2004). The overall trend suggests that boreholes with larger radii generate longer partially-emptied CBs.

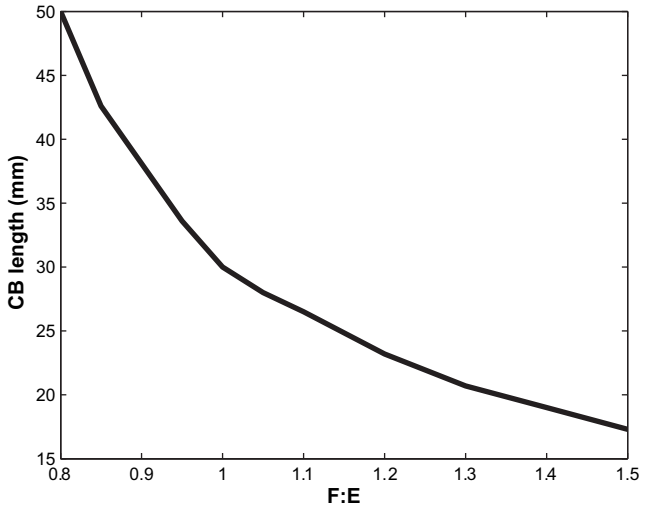

Fig. 7. Dependence of the final length of a partially-emptied compaction band developed in Mansfield Sandstone (Table 1) on the extent of its emptying by the fluid flow. The applied principal stresses are $\sigma_1 = 50$ MPa, $\sigma_2 = 30$ MPa , $\sigma_3 = 20$ MPa , and borehole radius is $R_{bor} = 11.5$ mm. Series of numerical simulations is conducted with different ratios of F:E (simulating different flow rates), and the resultant CB length is evaluated and plotted as a function of F:E ratio. The results demonstrate that when the F:E ratio grows (thus simulating a smaller flow rate), the total length (F + E) of partially-emptied CB decreases.

The calculations described above are repeated under the various borehole radii and loading conditions (as in Fig. 7 of Sheets and Haimson, 2004), and the results are summarized in Fig. 6 in comparison with the experimental results. The overall trend obtained from the numerical experiments proves the hypothesis that boreholes with larger radii generate longer partially-emptied CBs. However, it is seen from Fig. 6 that the model underestimates the experimental results at the small borehole radius, whereas it overestimates the experimental results at the large borehole radius. This feature can be explained by the fact that although flow rate was adjusted during the experiments, the ratio $F{:}E \cong 1$ varied slightly, from $F{:}E < 1$ for small borehole radii to $F{:}E > 1$ for large borehole radii.

4.2. The extent of CB emptying

These simulations are conducted with a borehole radius equal to $R_{bor} = 11.5$ mm and representative remote principal stresses $\sigma_1 = 50$ Mpa, $\sigma_2 = 30$ MPa, $\sigma_3 = 20$ MPa. As in the previous subsection, σ_{xx}, σ_{yy}, and σ_{zz} are calculated from Eqs. (4–6), while the yield function $f(\sigma_{ij})$ for Bentheim Sandstone (Baud et al., 2006) is calculated from (Eq. (8)). A series of numerical simulations were conducted with different ratios of *F:E* (simulating different flow rates) and the results are presented in Fig. 7. These results demonstrate that when the ratio *F:E* grows (addressing the case of lower flow rate), the total length $(F + E)$ of partially-emptied CB decreases. Although it is impossible to model directly the fluid flow in the current model, the obtained trend agrees with the trend demonstrated in Fig. 8 of Sheets and Haimson (2004), where under different loading conditions larger flow rates generate longer CBs characterized by smaller *F:E* ratios.

5. Discussion

Understanding mechanical behavior leading to slot breakouts in weak sandstones is fundamental in the efforts to efficiently extract water, petroleum, natural gas, and geothermal steam from wellbores. Formation of compaction bands ahead of breakouts reduces rock porosity, forming a narrow curtain of low permeability that could slow the free flow of fluids around wells. The induced elongated slot breakouts could be a source of unwanted sand production.

This work predicts analytically the expected final lengths of a type of slot-like borehole breakouts that are in effect partially-emptied compaction bands (Klaetsch and Haimson, 2002; Haimson, 2003; Haimson and Kovacich, 2003; Sheets and Haimson, 2004; Haimson, 2007; Haimson and Klaetsch, 2007) originating and propagating in anisotropic stress field. The analysis considers the partially-emptied CB's length dependence on borehole radius and on drilling fluid flow rate.

Fig. 6 demonstrates that under otherwise identical experimental conditions, a borehole with larger radius generates longer partially-emptied CBs. The stress components at the CB tip (t, Fig. 1), σ_{xx}, σ_{yy}, and σ_{zz}, are higher for the larger borehole radius (Eqs. (4–6)), due to the larger stresses around the emptied CB part (Eq. (5)) (stresses around the filled segment of CB remain unchanged as borehole radius grows, Eq. (4)). Substituting these stress components into Eqs.(7,8) yields a larger yield function for a longer borehole radius, and therefore longer partially-emptied CB. This analysis is in agreement with results of experiments (Haimson and Kovacich, 2003; Sheets and Haimson, 2004) studying the influence of the borehole radius on the final breakout length under different far-field stresses.

Concerning the second parameter, namely the influence of the extent of CB emptying, our model demonstrates that under otherwise equal far-field applied stresses and borehole radius, a larger *F:E* ratio (filled to emptied CB segments) yields a shorter total CB $(F + E)$, see Fig. 7. This tendency can be derived analyzing Eqs. (5a) and (5c) while assuming that the ratio *F:E* grows. Although the explicit flow rate is not incorporated directly in the current model, it is evident that larger flow rates evacuating more compacted matter from the emerging CBs, create smaller *F:E* ratios with larger stress concentrations around the emptied CB segment (stresses around the filled segment of CB remain unchanged, Eq. (4)), and eventually generate longer partially-emptied CBs. The emerging trend agrees with that demonstrated experimentally by Sheets and Haimson (2004), Fig. 8.

6. Conclusions

Boreholes are drilled into the Earth's crust under pre-existing in situ stress conditions. During or immediately after drilling, boreholes in high-porosity quartz-rich sandstones often develop slot-like breakouts that form as a consequence of stress-induced compactive rock failure. Compaction bands initiate at the borehole wall, at points subjected to the highest compressive stress concentration resulting from the pre-existing far-field stress. The debonded and often fragmented grains within the compaction band are totally or partially removed by the circulating drilling fluid, creating slot-shaped tabular breakouts. A new analytical model is developed here for studying the stress field around partially-emptied CBs and predicting the total lengths of these defects and their dependence on borehole radius and the extent of the CB emptying by the drilling-fluid flow. It was found theoretically that boreholes with larger radius generate longer partially-emptied CBs. The results also demonstrate that as the ratio of filled to emptied CB segments grows (addressing a smaller flow rate), the total length of partially-emptied CB decreases. Both theoretical results are in good agreement with results of the experiments conducted by Sheets and Haimson (2004).

Acknowledgments

Haimson's contribution was supported by the U.S. Office of Basic Energy Sciences, U.S. Department of Energy Grant DE-FG02-98ER14850. R. Sheets assisted with experimental work.

References

Baud, P., Vajdova, V., Wong, T.-F., 2006. Shear-enhanced compaction and strain localization: Inelastic deformation and constitutive modeling of four porous sandstones. Journal of Geophysical Research-Solid Earth 111, B12401.

Brace, W.F., Kohlstedt, D.L., 1980. Limits on lithospheric stress imposed by laboratory experiments. Journal of Geophysical Research 85 (B11), 6248–6252.

Brudy, M., Zoback, M.D., Fuchs, K., Rummel, F., Baumgartner, J., 1997. Estimation of the complete stress tensor to 8 km depth in the KTB scientific drill holes: Implications for crustal strength. Journal of Geophysical Research-Solid Earth 102 (B8), 18453–18475.

Cuss, R.J., Rutter, E.H., Holloway, R.F., 2003. Experimental observations of the mechanics of borehole failure in porous sandstone. International Journal of Rock Mechanics & Mining Sciences 40, 747–761.

Dresen, G., Stanchits, S., Rybacki, E., 2010. Borehole breakout evolution through acoustic emission location analysis. International Journal of Rock Mechanics and Mining Sciences 47, 426–435.

Haimson, B.C., 2003. Borehole breakouts in Berea sandstone reveal a new fracture mechanism. Pure and Applied Geophysics 160, 813–831.

Haimson, B.C., 2007. Micromechanisms of borehole instability leading to breakouts in rocks. International Journal of Rock Mechanics and Mining Sciences 44 (2), 157–173.

Haimson, B.C., Chang, C.D., 2002. True triaxial strength of the KTB amphibolite under borehole wall conditions and its use to estimate the maximum horizontal in situ stress. Journal of Geophysical Research-Solid Earth 107 (B10), 2257.

Haimson, B.C., Klaetsch, A., 2007. Compaction bands and the formation of slot-shaped breakouts in St. Peter sandstone. Rock Physics and Geomechanics in the Study of Reservoirs and Repositories 284, 89–105.

Haimson, B.C., Kovacich, J., 2003. Borehole instability in high-porosity Berea sandstone and factors affecting dimensions and shape of fracture-like breakouts. Engineering Geology 69, 219–231.

Haimson, B., Lin, W., Oku, H., Hung, J.-H., Song, S.-R., 2010. Integrating borehole-breakout dimensions, strength criteria, and leak-off test results, to constrain the state of stress across the Chelungpu Fault, Taiwan. Tectonophysics 482, 65–72.

Haimson, B.C., Song, I., 1998. Borehole Breakouts in Berea Sandstone: Two Porosity-dependent Distinct Shapes and Mechanisms of Formation. In: Proceedings of Conference on Rock Mechanics in Petroleum Engineering, vol. 1. Society of Petroleum Engineering, Richardson, TX, pp. 229–238.

Jaeger, J.C., Cook, N.G.W., 1976. Fundamentals of Rock Mechanics. Chapman and Hall, London.

Katsman, R., Aharonov, E., 2006. A study of compaction bands originating from cracks, notches, and compacted defects. Journal of Structural Geology 28 (3), 508–518.

Katsman, R., Aharonov, E., Scher, H., 2006a. A numerical study on localized volume reduction in elastic media: some insights on the mechanics of anticracks. Journal of Geophysical Research-Solid Earth 111, B03204.

Katsman, R., Aharonov, E., Scher, H., 2006b. Localized compaction in rocks: Eshelby's inclusion and the Spring Network Model. Geophysical Research Letters 33 (10), L10311.

Katsman, R., Aharonov, E., Haimson, B., 2009. Compaction bands induced by borehole drilling. Acta Geotechnica 4, 151–212.

Klaetsch, A.R., Haimson, B.C., et al., 2002. Peter sandstone. In: Hammah, R. (Ed.), Porosity-dependent Fracture-like Breakouts in St Mining and Tunneling Innovation and Opportunity. University of Toronto Press, pp. 1365–1371.

Klein, E., Baud, P., Reuschle, T., Wong, T.-F., 2001. Mechanical behaviour and failure mode of Bentheim sandstone under triaxial compression. Physics and Chemistry of the Earth Part A- Solid Earth and Geodesy 26 (1–2), 21–25.

Mollema, P.N., Antonellini, M.A., 1996. Compaction bands: a structural analog for anti-mode I cracks in aeolian sandstone. Techtonophysics 267 (1–4), 209–228.

Murakami, Y., 1987. Stress Intensity Factors Handbook. Pergamon, Oxford.

Scholz, C.H., 2000. The Mechanics of Earthquakes and Faulting. Cambridge University Press.

Sheets, R. J., Haimson, B. C., 2004. Drilling variables affecting fracture-like borehole breakout characteristics. In: Gulf Rocks 2004, reviewed CD-Rom Proceedings, paper ARMA/NARMS 04–484.

Song, I., Haimson, B.C., 1997. Polyaxial strength criteria and their use in estimating in situ stress magnitudes from borehole breakout dimensions. International. Journal of Rock Mechanics and Mining Sciences 34 (3–4), 116.

Sternlof, K.R., Rudnicki, J.W., Pollard, D.D., 2005. Anticrack inclusion model for compaction bands in sandstone. Journal of Geophysical Research-Solid Earth 110 (B11), B11403.

Tembe, S., Vajdova, V., Wong, T.-F., Zhu, W., 2006. Initiation and propagation of strain localization in circumferentially notched samples of two porous sandstones. Journal of Geophysical Research-Solid Earth 111 (B2), B02409.

Townend, E., Thompson, B.D., Benson, P.M., Meredith, P.G., Baud, P., Young, R.P., 2008. Imaging compaction band propagation in Diemelstadt sandstone using acoustic emission locations. Geophysical Research Letters 35, L15301.

Vajdova, V., Wong, T.-F., 2003. Incremental propagation of discrete compaction bands: acoustic emission and microstructural observations on circumferentially notched samples of Bentheim. Geophysical Research Letters 30 (14), 1775.

Vajdova, V., Wong, T.-F., Farell, D. E., Issen, K. A., Challa, V., 2003. Experimental observation and numerical simulation of initiation and propagation of compaction bands in a sandstone. Proceedings ASCE Engineering Mechanics Conference, Seattle, July 16–18.

Vernik, L., Zoback, M.D., 1992. Estimation of maximum horizontal principal stress magnitude from stress-induced well bore breakouts in the cajon pass scientific-research borehole. Journal of Geophysical Research-Solid Earth 97 (B4), 5109–5119.

Wong, T., David, C., Zhu, W., 1997. The transition from brittle faulting to cataclastic flow in porous sandstones: mechanical deformation. Journal of Geophysical Research-Solid Earth 102, 3009–3025.